ACS OMEGA

http://pubs.acs.org/journal/acsodf

Article

Modification of the Calculation Method for Dynamic Reserves in Tight Sandstone Gas Reservoirs

Jie He, Xiangdong Guo, Hongjun Cui, Kaiyu Lei, Yanyun Lei, Lin Zhou, Qinghai Liu, Yushuang Zhu,* and Linyu Liu

Cite This: *ACS Omega* 2021, 6, 29955−29964

ABSTRACT: The determination of dynamic reserves is important for tight sandstone gas reservoirs in production. Based on the geological and gas data of the Yan'an gas field, the influence of pressure on the properties of natural gas is studied by mathematical methods. At the same time, the modified flowing material balance equation is established considering the changes in gas viscosity and compressibility. The result shows that (1) the viscosity of natural gas increases rapidly with pressure; (2) the deviation factor decreases with pressure (P < 15 MPa) and then increases (P > 15 MPa) with temperature; (3) the compressibility decreases rapidly with pressure and increases with temperature; (4) compared with the results of the material balance method, the average error of the flowing material balance method is 33.95%, and the accuracy of the modified flowing material balance method is higher with an average error of 1.25%; and (5) a large change in the production will affect the accuracy of the modified flowing material balance method, especially a shut-in for a long time before the pressure drop production is calculated at a certain time, so data points that are relatively consistent should be selected as far as possible to calculate the dynamic reserves. The findings of this study can help in the accurate evaluation of dynamic reserves of the tight gas reservoir in the Yan'an gas field and are an important guide for the formulation of a rational plan for the gas reservoir and its economic and efficient development.

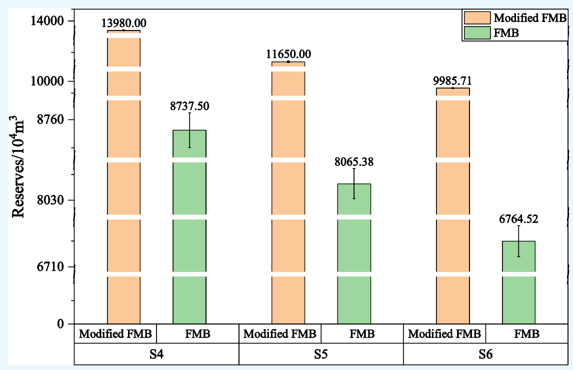

1. INTRODUCTION

The Yan'an gas field, located in the southeast of Yishan slope in the Ordos basin, is a typical tight sandstone reservoir with the characteristics of low permeability, strong heterogeneity, strong stress sensitivity, and a complex percolation mechanism.[1,2] Pressure measurement and variable production often occur in the process of production, therefore, it is difficult to calculate the dynamic reserves in the gas field.[3,4]

At present, the main methods for calculating dynamic reserves including the material balance method, production decline method, production accumulation method, elastic two-phase method, and the advantages and disadvantages of each method are shown in Table 1[5−8]

When there is a lack of data such as bottom pressure or the well produces serious amount of water, the MBM has a large error.[9−11] Mattar put forward the FMB (flowing material balance) method, which is analyzed from the point of view of percolation mechanics.[12] Sun et al. combined the material balance equation and the pressure distribution characteristics at different production stages to establish a completely new production prediction model.[5] These methods do not take into account the effect of pressure on the viscosity and compressibility of gas, that is, it is considered that the viscosity and compressibility of natural gas remain unchanged.[13]

Table 1. Advantages and Disadvantages of Each Method[a]

method	advantages	disadvantages
MBM	the most accurate	less data is required, and abnormal data can cause great errors.
PDM	predict gas production, powerful function	accurately determine the type of decrement
PAM	more accurate and easy to operate	not applicable in the early stages of development
ETM	no need for shut-in pressure measurement data	inaccurate results at low permeability reservoirs

[a]MBM: material balance method; PDM: production decline method; PAM: production accumulation method; ETM: elastic two-phase method.

However, when the formation pressure of the reservoir is low, the assumption is not valid, so there is an error in the calculation.[2]

Received: August 17, 2021
Accepted: October 13, 2021
Published: October 29, 2021

https://doi.org/10.1021/acsomega.1c04473
ACS Omega 2021, 6, 29955−29964

To solve the above problems, a modified FMB is proposed in this study. For a closed reservoir that has been produced for a period of time, the pressure is transmitted to the boundary of the formation and seepage enters a pseudo-steady-state.[14] As shown in Figure 1, the pressure curve will be parallel, and the formation pressure drop is almost equal to the bottom flow pressure drop in the same time.[15,16] The FMB method is to replace the formation pressure with the wellhead casing pressure and bottom flow pressure, and the modified FMB method is to increase the influence of pressure on the viscosity and compressibility on the basis of the FMB method. Finally, this method is verified by data from the tight reservoir in the Yanchang gas field in the Ordos basin.

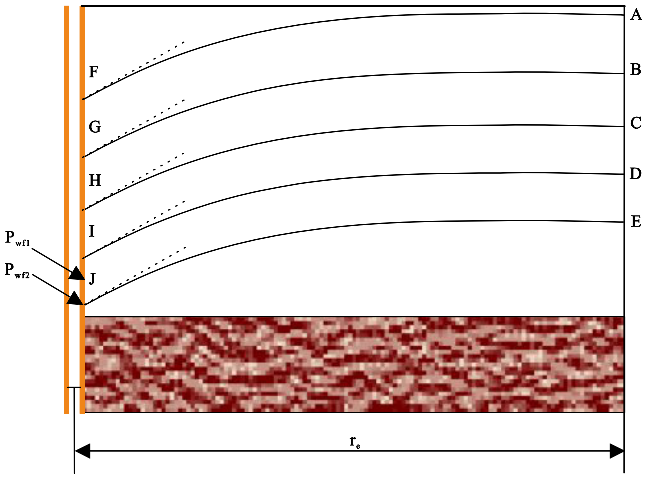

Figure 1. Pressure profile of the well.

1.1. GEOLOGICAL BACKGROUND

Ordos basin is a large sedimentary basin with multicycle evolution and multisedimentary types.[17] The area of the basin is about 25 × 10^4 km^2. At present, the structure is a large syncline with slow width in the east and steep in the west, and the dip angle is generally less than 1°. Fault folds in the margin of the basin are developed and the internal structure is relatively simple.[18] There is no secondary structure in the basin, and the tertiary structure is dominated by nose uplift, and there are few anticline structures with a large amplitude and good trap.[19] According to the current structural shape, basement properties, and structural characteristics of the basin, the Ordos basin can be divided into six first-order structural units: Yimeng uplift, Weibei uplift, western Shanxi flexure fold belt, Yishan slope, Tianhuan depression, and western margin thrust structural belt.

The Yan'an gas field is located in the southeast of Yishan slope in the Ordos basin, as shown in Figure 2[20] The comprehensive geological study shows that the Upper Paleozoic in the study area has many favorable conditions, which are beneficial to the formation and enrichment of large lithologic gas reservoirs.[21]

A total of 689 wells are divided into three types according to the OFR (open flow rate), and the results are shown in Table 2.

2. METHODS

2.1. Property of Natural Gas. *2.1.1. Viscosity of Natural Gas.* Through 20 samples provided in the Supporting Information under the condition of temperature (352 K) and pressure (30 MPa) (Table S1), the relationship between pressure and viscosity is drawn based on the calculated results. As shown in Figure 3, the viscosity increases with the temperature under the condition of low pressure and decreases with temperature when the pressure is greater than 10 MPa.[22] The viscosity increases with the pressure whether the pressure is low or high.[23]

2.1.2. Deviation Factor of Natural Gas. The deviation factor refers to the ratio of the real volume to the ideal volume of the same mass gas under a certain temperature and pressure, and the relationship between Z at different temperatures is shown in Figure 4[24] When the pressure is lower than 15 MPa, Z decreases with the pressure and then increases with the temperature.

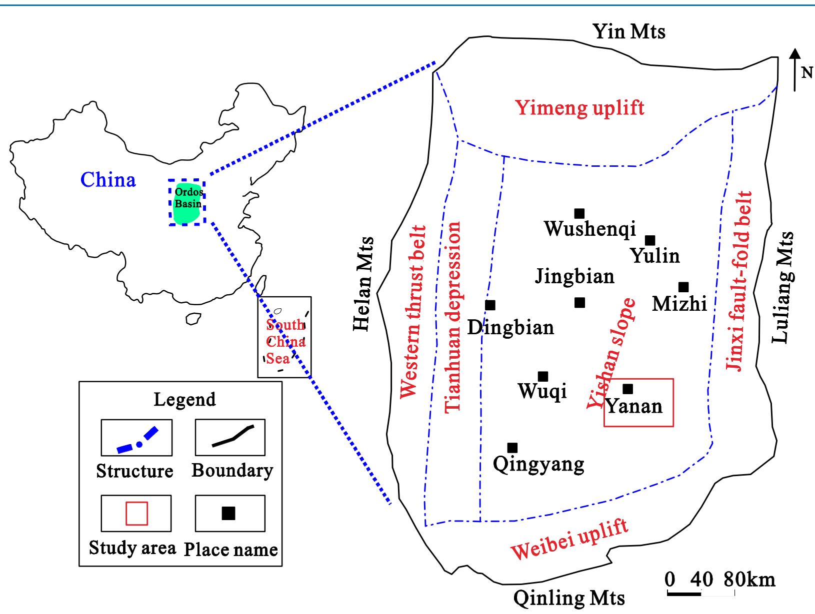

Figure 2. Location of the Yan'an gas field in the Ordos basin.

https://doi.org/10.1021/acsomega.1c04473
ACS Omega 2021, 6, 29955−29964

Table 2. Classification Results of Wells in the Study Area[a]

	OFR > 10 × 10^4 m^3/day		4 < OFR < 10 × 10^4 m^3/day		OFR < 4 × 10^4 m^3/day	
classification basis	type-I		type-II		type-III	
number	well	proportion (%)	well	proportion (%)	well	proportion (%)
	194	31.36	134	20.05	361	48.59

[a]OFR: open flow rate.

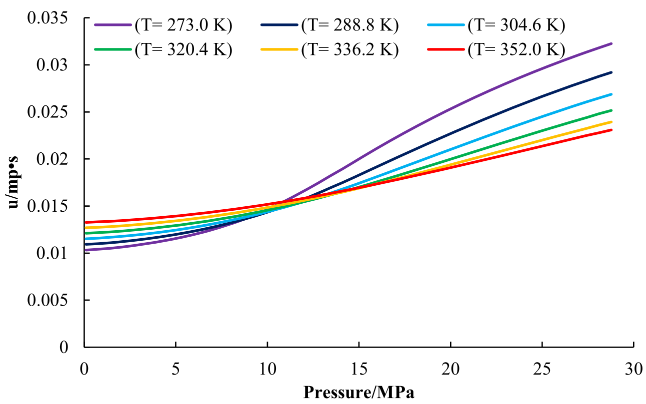

Figure 3. $P \sim \mu$ curve of natural gas.

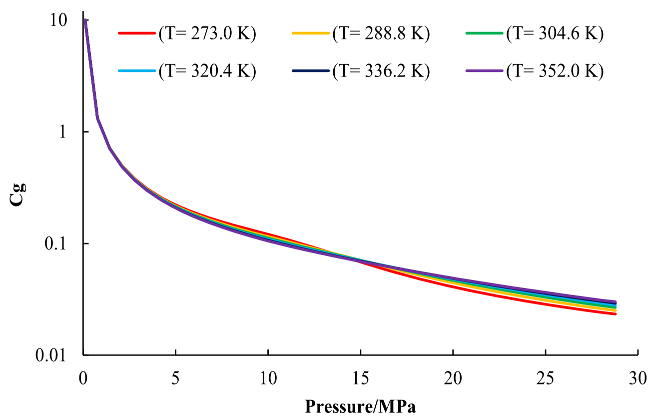

Figure 5. P–C_g curve of natural gas.

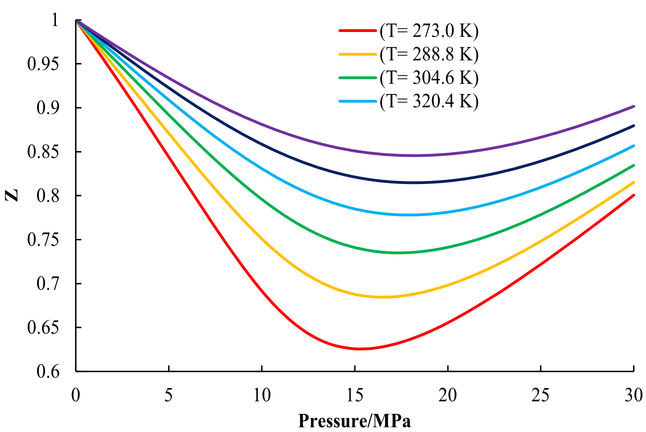

Figure 4. P–Z curve of natural gas.

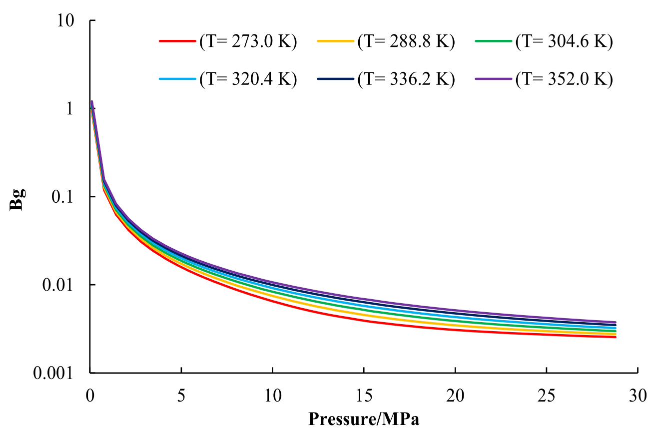

Figure 6. P–B_g curve of natural gas.

2.1.3. Compressibility of Natural Gas. Compressibility refers to the change of unit volume with pressure under the condition of constant temperature.

According to the data of 20 samples, P–C_g at different temperatures can be obtained, as shown in Figure 5, and the compressibility decreases with temperature and pressure and is less affected by temperature.

2.1.4. Volume Factor of Natural Gas. The volume factor is measured under the surface standard conditions, so it is necessary to convert the volume of natural gas measured under the surface conditions to the volume under the formation conditions.[25,26] This conversion coefficient is the volume factor of natural gas. As shown in Figure 6, the volume factor decreases with the pressure and increases with the temperature.

2.2. FMB Method. For the reservoir produced by a circular, closed, and central vertical well, when it enters the pseudo-steady-state, then[27]

$$\frac{\partial(\overline{P}/\overline{u_g}\overline{C_g}\overline{Z})}{\partial G_p} = \frac{\partial(\overline{P_{wf}}/u_{gwf}c_{gwf}\overline{Z}_{wf})}{\partial G_p} \qquad (1)$$

In the FMB method, it is assumed that the pressure has no effect on the viscosity and compressibility of gas

$$\partial(\overline{u_g c_g}) = \partial(u_{gwf}c_{gwf}) \qquad (2)$$

$$\frac{\partial(\overline{P}/\overline{Z})}{\partial G_p} = \frac{\partial(\overline{P}_{wf}/\overline{Z}_{wf})}{\partial G_p} \qquad (3)$$

Therefore, when the reservoir reaches the pseudo-steady-state, $\overline{P}/\overline{Z} \sim G_p$ is parallel to $P_{wf}/Z_{wf} \sim G_p$ in Cartesian coordinates. According to the P_{wf}/Z_{wf} and G_p data in production, the data showing a straight line are fitted, and then a parallel line is made through P_i/Z_i, and the intercept of the parallel line on G_p is the dynamic reserve G_i.

2.3. Modified FMB Method. The results are shown in Figures 3–6. It can be seen that the viscosity, compressibility, and deviation factor change obviously with pressure.

It can be seen that eq 2 is not valid according to the relationship between $\mu_g \cdot C_g$ and P from Figure 7, that is, the viscosity and compressibility vary with pressure.

As can be seen from Figure 7

https://doi.org/10.1021/acsomega.1c04473
ACS Omega 2021, 6, 29955−29964

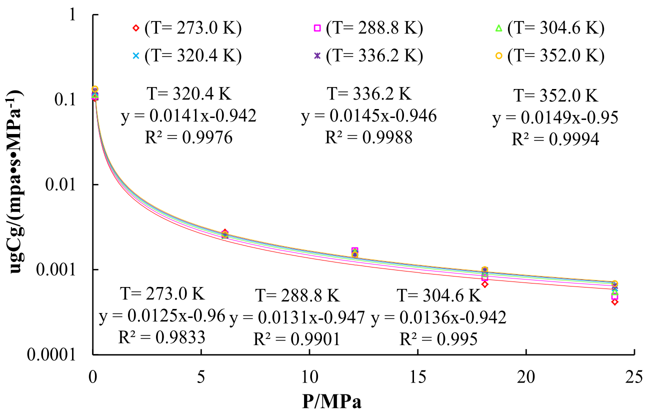

Figure 7. $P \sim \mu_g c_g$ curve of natural gas.

$$|\partial(\overline{u_g c_g})| < |\partial(u_{gwf} c_{gwf})| \tag{4}$$

It can be seen that the slope of $P_{wf}/Z_{wf} \sim G_p$ is greater than that of $\overline{P}/\overline{Z} \sim G_p$. Therefore, reserves determined by the FMB method are smaller than the real.

From eq 3

$$\frac{\partial(\overline{P}/\overline{Z})}{\partial G_p} = \frac{\partial(\overline{u_g}\overline{C_g})}{\partial(u_{gwf} c_{gwf})} \frac{\partial(P_{wf}/Z_{wf})}{\partial G_p} \tag{5}$$

where $\overline{P_{pss}}$ and $P_{wf\text{-}pss}$ represent the average formation pressure and bottom flow pressure at the initial stage of the pseudo-steady-state, respectively. In the pseudo-steady-state, the average formation pressure and bottom flow pressure decrease at the same speed, so it can be considered that λ remains unchanged. At the same time, λ can be calculated by the $P_{wf\text{-}pss}$ values of $\mu_g c_g$ and $\overline{P_{pss}}$ at the initial stage of the pseudo-steady-state

$$\frac{\partial(\overline{u_g}\overline{C_g})}{\partial(u_{gwf} c_{gwf})} \approx \frac{(u_g C_g)|_{\overline{P_{pss}}}}{(u_g C_g)|_{P_{wf-pss}}} \approx \frac{(u_g C_g)|_{P_i}}{(u_g C_g)|_{P_{wf-pss}}} = \lambda$$

$$\frac{\partial(\overline{P}/\overline{Z})}{\partial G_p} = \lambda \frac{\partial(P_{wf}/Z_{wf})}{\partial G_p} \tag{6}$$

Based on the process, steps of the modified FMB method are as follows (Figure 8)

(1) $(u_g c_g)|_{pi}$ and $(u_g c_g)|_{P_{wf-pss}}$ are determined according to $p \sim \mu_g c_g$ and λ is calculated according to eq 6.

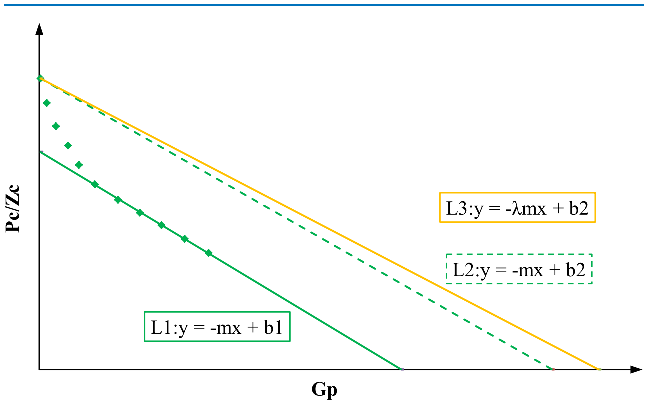

Figure 8. Dynamic reserves determined by modified FMB.

(2) The $P_{wf}/Z_{wf} \sim G_p$ curve and the slope *-m* can be obtained by the bottom flow pressure and cumulative production data.

(3) Take $-\lambda m$ as the slope and make a straight line over P_i/Z_i, and the intercept is the reserve determined by modified FMB (modified G_i).

(4) Similarly, P_c can be used to replace P_{wf}.

3. RESULTS

3.1. Type-I Wells. The initial production of type I in the Yan'an gas field is high, the pressure drops slowly, and the time of stable production is long, so it has a good production capacity under the condition of low pressure.

S-4 well is a typical type I in the study area, and the OFR is 26.57×10^4 m^3/day. It has been in production since August 2013. It can be seen that the average monthly production is 64 $\times 10^4$ m^3/m from Figure 9, and the water production is at a low level, with an average monthly production of 4.28 m^3/m, and the water−gas ratio is maintained at 0.066 ($m^3/10^4$ m^3) at the initial stage (August 2013−April 2015). In the second stage (May 2015−April 2017), the casing pressure and the oil pressure decrease rapidly, resulting in a decline in production and an increase in water production. In the third stage (May 2017−April 2020), the monthly gas and water production are kept at a low level, the casing pressure is about 7 MPa, and the oil pressure is about 8 MPa. Up to now, the cumulative production of S-4 is 3633.775×10^4 m^3 and the cumulative water production is 356.67 m^3.

As shown in Figure 10, the linear fitting is carried out and the slope of the straight line is −0.0024 according to the relationship between P_c/Z_c and G_p. A straight line is obtained from this slope and the P_i/Z_i point, and the intercept is 0.8737 $\times 10^8$ m^3, which is the dynamic reserve of S-4 determined by FMB.

The results show that $-\lambda = -0.6387$ and $-\lambda m = -0.0015$. Considering $-\lambda m$ as the slope and making a straight line through the P_i/Z_i point, the intercept is 1.398×10^8 m^3, which is the dynamic reserve of S-4 determined by modified FMB.

3.2. Type-II Wells. S-5 well belongs to type II (Figure 11). One-hundred ninety days of the trial production operation was carried out from November 19, 2009, to May 27, 2010, and 70 days of the pressure recovery test was carried out from May 27 to August 7, 2010. The OFR is 4.705×10^4 m^3/day, and the original formation pressure is 25.872 MPa. The production starts at 1.5×10^4 m^3/day and it is difficult to be unchanged due to the large pressure fluctuation in the trial production process. Thus, the daily production is gradually reduced to about 1×10^4 m^3/day and the daily water production is 0.1−1.8 m^3/day. After that, the oil pressure decreases from 14.41 to 12.36 MPa at a decline rate of 0.051 MPa/day, which shows that the production is basically constant. Up to April 2020, the cumulative production is 3471.62×10^4 m^3, and the cumulative water production is 490.25 m^3.

As shown in Figure 12, the slope of the straight line is −0.0026 in the $P_c/Z_c \sim G_p$ curve. A line is obtained from this slope and the P_i/Z_i point, and the intercept is 0.8065×10^8 m^3, which is the dynamic reserve of S-5 determined by FMB.

The calculation results show that $-\lambda = -0.704$ and $-\lambda m = -0.0018$. Considering $-\lambda m$ as the slope and making a straight line through the P_i/Z_i point, the intercept is 1.1650×10^8 m^3, which is the dynamic reserve of S-5 determined by modified FMB.

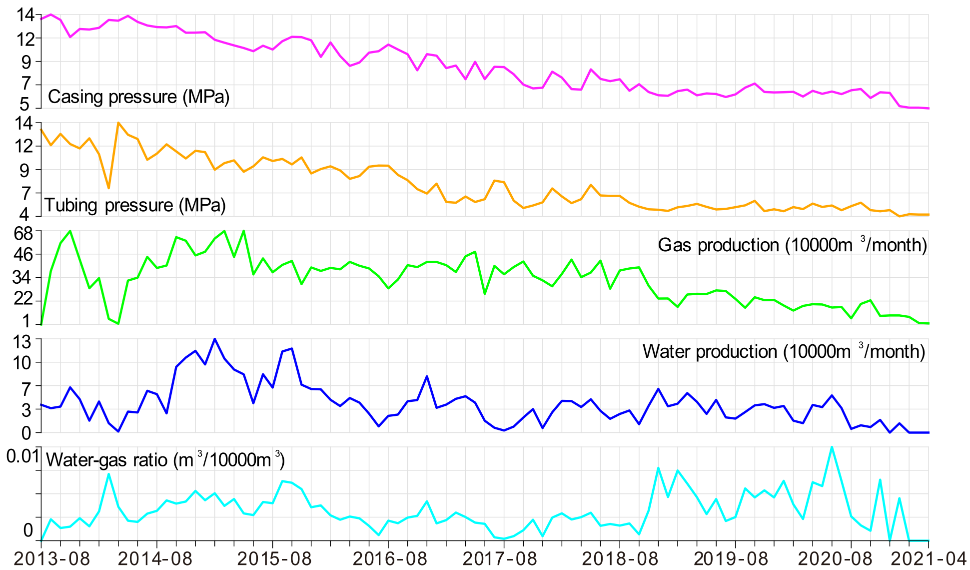

Figure 9. Production curve of S-4.

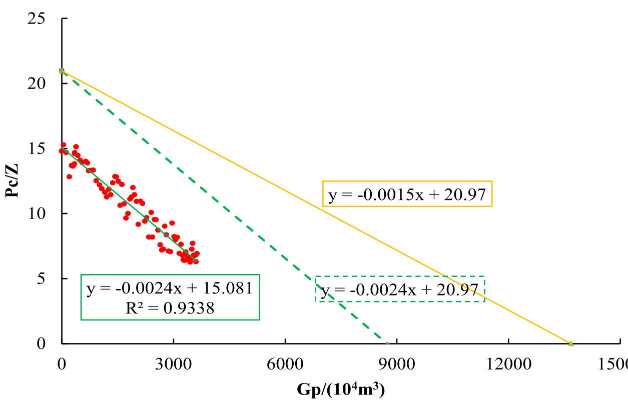

Figure 10. Results of S-4 by modified FMB.

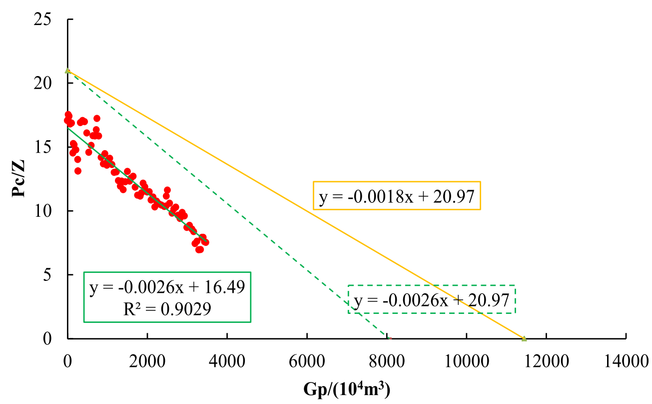

Figure 12. Results of S-5 by modified FMB.

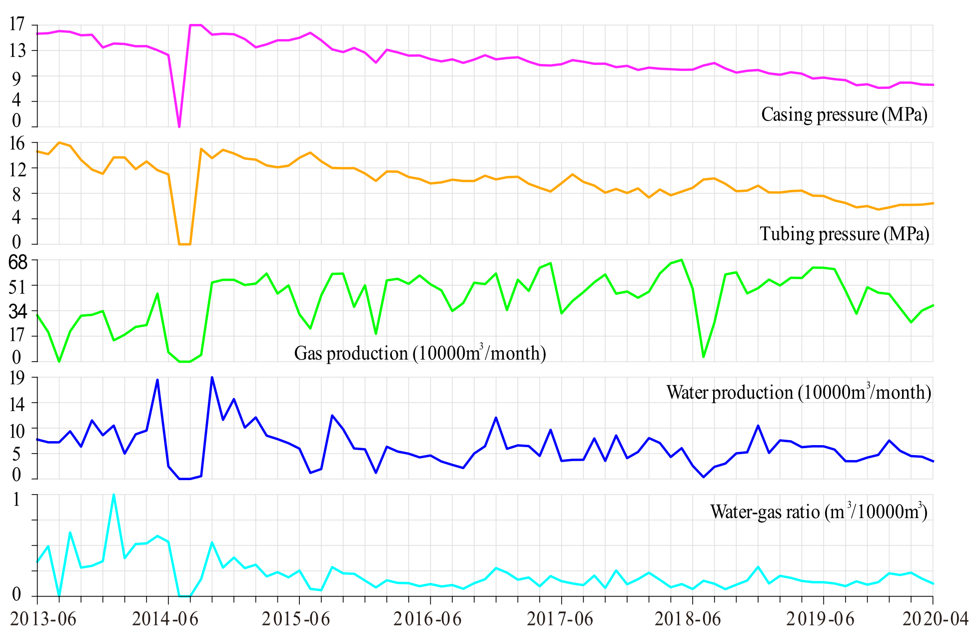

Figure 11. Production curve of S-5.

https://doi.org/10.1021/acsomega.1c04473
ACS Omega 2021, 6, 29955−29964

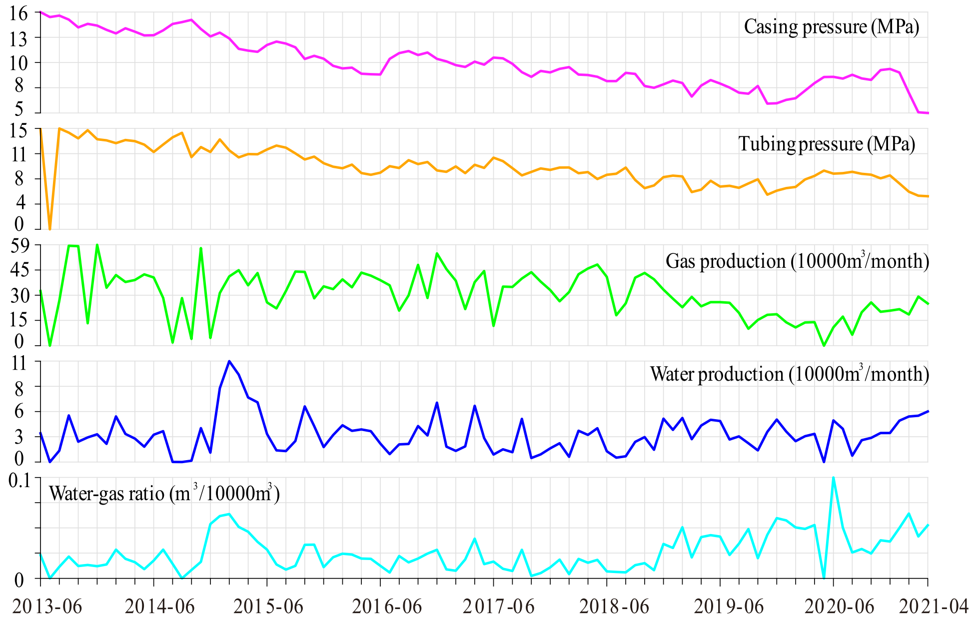

Figure 13. Production curve of S-6.

3.3. Type-III Wells.

S-6 well is one of type III, and the OFR is 8.944 × 10^4 m^3/day. It can be seen that the average production of S-6 is 50 × 10^4 m^3/m at the initial stage from Figure 13(June 2013−December 2014). The water production is at a low level, the average monthly production is 3.02 m^3/m, and the water−gas ratio is maintained at 0.060 $m^3/10^4$ m^3. The casing pressure decreases rapidly and the monthly production remains unchanged in the second stage (from January 2015 to June 2018). In the third stage (July 2018−April 2020), the monthly production decreases rapidly due to the high water production rate. Up to now, the cumulative production of S-6 is 2580.92 × 10^4 m^3, and the cumulative water production is 237.55 m^3.

As shown in Figure 14, the linear fitting is carried out and the slope of the straight line is −0.0031 according to the relationship between P_c/Z_c and G_p. A straight line is obtained from this slope and the P_i/Z_i point, and the intercept is 0.6765 × 10^8 m^3, which is the dynamic reserve of S-6 determined by FMB.

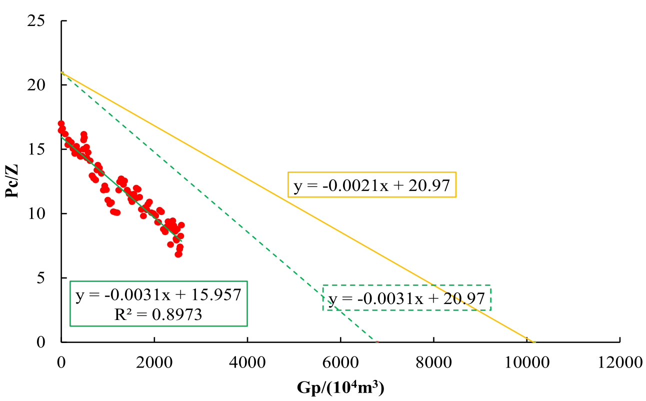

Figure 14. Results of S-6 by modified FMB.

The calculation results show that $-\lambda = -0.667$ and $-\lambda m = -0.0021$. Considering $-\lambda m$ as the slope and making a straight line through the P_i/Z_i point, the intercept is 0.9986 × 10^8 m^3, which is the dynamic reserve of S-6 determined by modified FMB.

4. DISCUSSION

Compared with the other methods, the MBM is more reliable during calculation with the average formation pressure.

4.1. Method Verification.

Based on the measured formation pressure at different stages of the production, the relationship between the cumulative production and P/Z is shown in Table 3 and Figures 15−17.

It can be obtained from Table 4 and Figure 18 that (1) the dynamic reserve of S-4 is 1.3849 × 10^8 m^3 calculated by the MBM. By comparing the above results, the error of FMB is 36.91%, and the error of modified FMB is 0.95%; (2) the dynamic reserve S-5 is 1.1864 × 10^8 m^3 calculated by the MBM, therefore, the error of FMB is 32.02% and the error of modified FMB is 1.80%; and (3) the dynamic reserve of S-6 is 1.0086 × 10^8 m^3 calculated by the MBM; obviously, the error of FMB is 32.93%, and the error of modified FMB is 1.00%. Therefore, compared with FMB, the error of modified FMB is small, with an average of 1.25%.

4.2. Advantages and Disadvantages.

Three methods are used to calculate the dynamic reserve of 33 wells in the study area, and the results are shown in Table 5. The average reserves calculated by the MBM and the FMB are 1.2731 × 10^8 m^3 and 0.6794 × 10^8 m^3, respectively. The minimum error is 28.499%, the maximum is 58.816%, and the average is 44.536%. The average reserve of modified FMB is 1.3008 × 10^8 m^3, the minimum error is 1.290%, the maximum value is 3.063%, and the average is 2.114%. It is worth noting that the wells with large errors in the calculation results of modified FMB are S-56 and S-60-1.

Combined with the production, S-56 was put into production in June 2013 (Figure 19), and the state of shut-in appeared intermittently from June 2013 to December 2016, the pressure recovery state was in a short time, which reflected that the formation pressure and casing pressure drop in the early stage were relatively small, and the production per unit pressure drop was relatively large because there was no

Table 3. Pressure Measured of Three Wells

time	S4 G_p (10^4 m^3)	S4 P (MPa)	S4 P/Z	S5 G_p (10^4 m^3)	S5 P (MPa)	S5 P/Z	S6 G_p (10^4 m^3)	S6 P (MPa)	S6 P/Z
201 312	268.355	18.800	20.567	135.008	18.923	20.727	216.712	18.713	20.515
201 406	434.815	18.276	20.018	265.966	18.386	20.091	450.907	18.281	20.023
201 412	787.525	17.918	19.589	431.721	18.147	19.893	546.945	17.644	19.321
201 506	1211.685	17.617	19.152	720.386	17.578	19.273	767.195	17.980	19.659
201 512	1522.465	16.668	18.186	990.256	17.360	18.988	971.055	16.738	18.231
201 606	1836.965	16.488	17.915	1278.196	16.565	18.069	1200.765	16.678	18.048

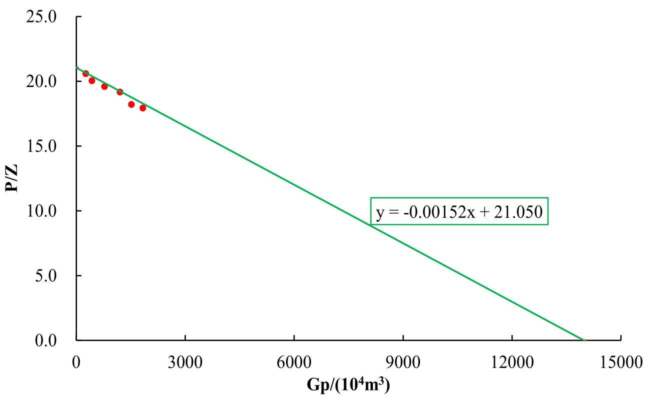

Figure 15. Results of S-4 by the MBM.

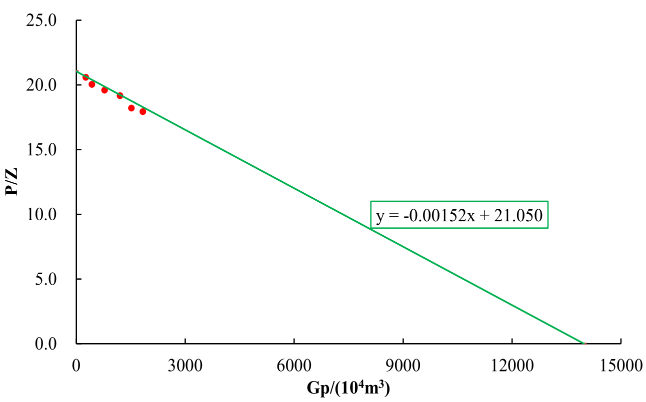

Figure 16. Results of S-5 by the MBM.

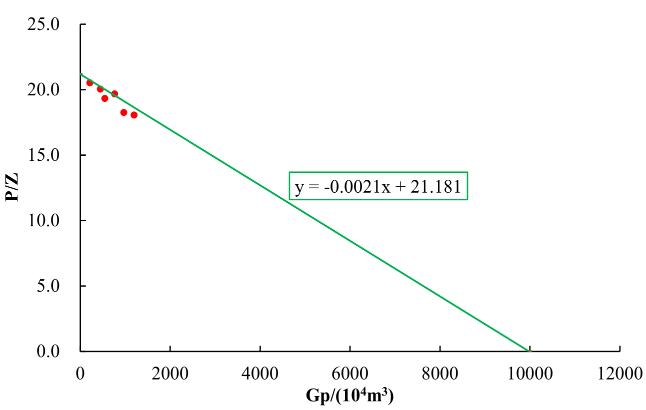

Figure 17. Results of S-6 by the MBM.

intermittent shut-in in the later stage. Therefore, it can be concluded that the early shut-in leads to large dynamic reserves. Similarly, S-60-1 was put into production in July 2015 (Figure 20), and the intermittent shut-in occurred in the later

Table 4. Results of FMB and Modified FMB

well	MBM (10^4 m^3)	FMB (10^4 m^3)	error (%)	modified FMB (10^4 m^3)	error (%)
S4	13848.68	8737.50	36.91	13980.00	0.95
S5	11864.04	8065.38	32.02	11650.00	1.80
S6	10086.19	6764.52	32.93	9985.71	1.00
average	11932.97	7855.80	33.95	11871.90	1.25

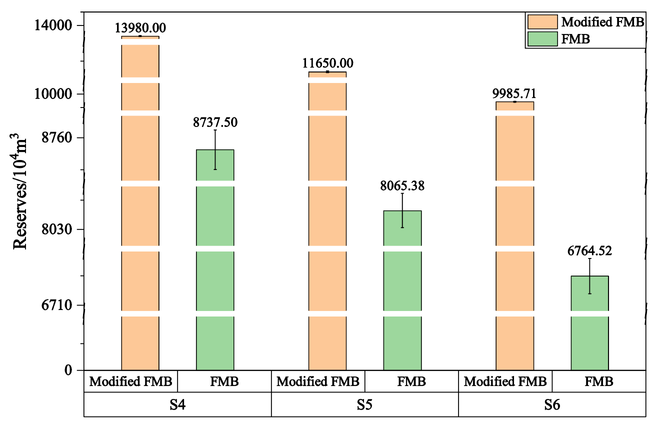

Figure 18. Error of dynamic reserves.

stage, and the production law could not fully reflect the real state, resulting in a large error.

To sum up, the new method established also has limitations. The accuracy of the calculation of the modified FMB would be affected when the production changes greatly, especially a shut-in for a long time before calculating the production of pressure drop at a certain time. Therefore, data that are relatively consistent should be selected as far as possible to calculate the dynamic reserves.

5. CONCLUSIONS

Considering the viscosity, compressibility, and deviation coefficient of natural gas, the FMB method is modified, and the calculation method and steps are given in this study. At the same time, verified by the production data of typical wells, the results show that compared with the results of the MBM, the average error of the FMB method is 33.95%, and the average error of the modified FMB method is 1.25%. Therefore, the modified FMB method is more accurate in calculating dynamic reserves.

In addition, with conventional methods, there is a large error in the model created when there is a longer shut-in operation. It is believed that the mathematical model is a good starting for future research on dynamic reserves in the field of an unconventional reservoir, and this theoretical design is expected to be applied in other simulation methods for gas

https://doi.org/10.1021/acsomega.1c04473
ACS Omega 2021, 6, 29955−29964

Table 5. Results of Three Dynamic Reserve Methods

WELL	initial wellhead casing pressure (MPa)	pseudo-steady wellhead casing pressure (MPa)	MBM reserves (10^4 m^3)	FMB reserves (10^4 m^3)	FMB error (%)	modified FMB reserves (10^4 m^3)	modified FMB error (%)
S1	15.8462	12.8592	7153.74	4282.75	40.133	7342.40	2.637
S12	17.1079	13.4597	14 160.04	6336.27	55.252	14 370.62	1.487
S14	18.7003	12.8507	10 602.13	5843.84	44.881	10 833.20	2.179
S15	17.3198	14.2056	12 111.63	8659.90	28.499	12 334.85	1.843
S16	18.0042	14.2344	12 881.02	6668.23	48.232	13 183.31	2.347
S18	20.9695	14.9531	9300.99	5114.52	45.011	9482.64	1.953
S19	19.1588	13.4765	15 158.98	7982.84	47.339	15 426.74	1.766
S2	16.6048	12.7247	4488.28	2515.88	43.946	4560.57	1.611
S20	20.9194	15.9530	23 281.23	11 621.87	50.081	23 693.58	1.771
S23	17.2632	12.3611	18 463.87	11 508.79	37.669	18 979.53	2.793
S24	17.8761	13.3496	8295.53	4831.38	41.759	8488.67	2.328
S3	15.3464	11.4357	4419.17	3009.09	31.908	4498.07	1.785
S36	16.7579	13.4424	14 231.18	9857.57	30.733	14 547.33	2.222
S37	20.8429	15.2572	8776.13	4631.75	47.223	8951.42	1.997
S38	15.3464	12.7981	17 870.36	10 961.70	38.660	18 146.58	1.546
S39	16.4099	11.9387	7545.85	3907.11	48.222	7699.04	2.030
S40	20.4163	15.6005	8117.51	3343.29	58.814	8310.90	2.382
S41	17.7460	12.0839	9631.05	5070.29	47.355	9871.88	2.500
S42	20.1747	15.6066	12 423.66	5933.73	52.239	12 605.25	1.462
S47	15.4740	11.0778	9600.02	5951.53	38.005	9782.98	1.906
S48	19.7822	14.7414	8301.62	5187.84	37.508	8495.94	2.341
S53	18.1943	13.6024	10 815.71	6273.89	41.993	11 010.45	1.801
S53-1	16.5886	14.4144	3168.25	1987.80	37.259	3213.64	1.433
S56	17.5138	14.1972	7124.17	4230.08	40.623	7339.25	3.019
S60	22.6343	17.3155	12 818.85	5956.40	53.534	12 984.22	1.290
S60-1	23.8290	15.3464	14 704.97	7073.23	51.899	15 155.41	3.063
S8	17.9103	13.5156	62 126.78	25 586.07	58.816	63 747.11	2.608
Y170	17.9788	14.2530	16 910.98	11 236.74	33.554	17 356.94	2.637
Y185	19.8759	13.2931	2211.32	1129.31	48.930	2257.58	2.092
Y196	18.4994	10.9542	19 406.76	9736.50	49.829	19 839.12	2.228
Y202	18.1875	13.3156	8538.40	4208.89	50.706	8750.41	2.483
Min	15.3464	10.9542	2211.32	1129.31	28.499	2257.58	1.290
Max	23.8290	17.3155	62 126.78	25 586.07	58.816	63 747.11	3.063
Average	18.3638	13.6973	12 730.33	6794.81	44.536	13 008.37	2.114

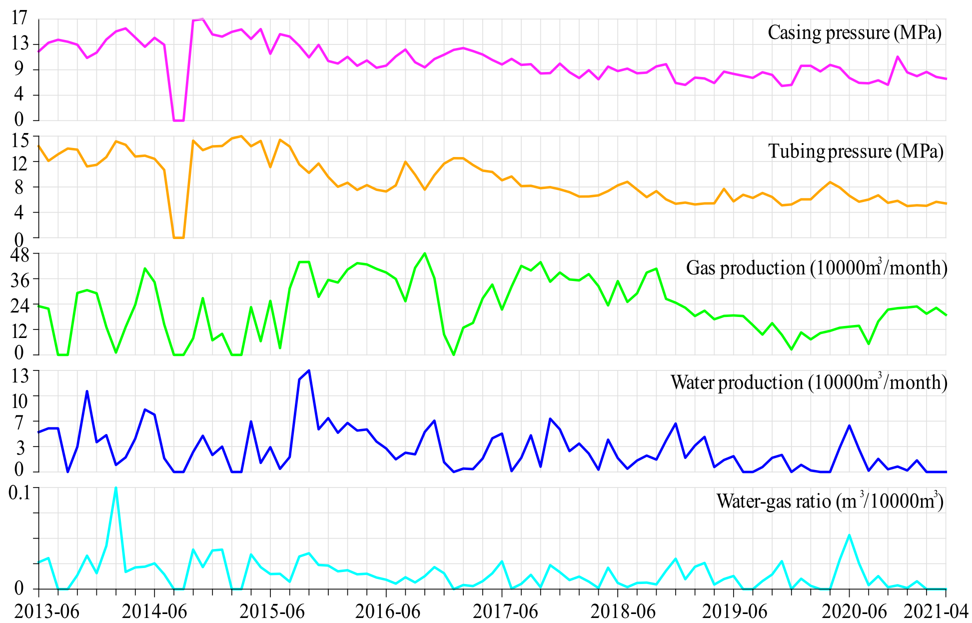

Figure 19. Production curve of S-56.

https://doi.org/10.1021/acsomega.1c04473
ACS Omega 2021, 6, 29955−29964

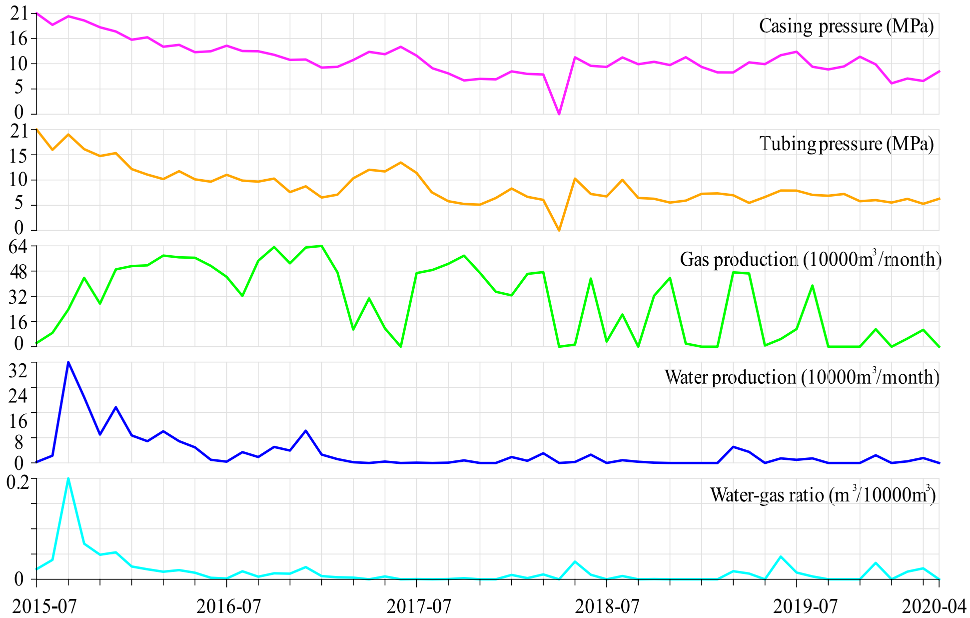

Figure 20. Production curve of S-60-1.

(shale gas, coalbed methane) and multimedia (matrix, fracture, and cavity) reservoirs.

■ ASSOCIATED CONTENT

Supporting Information

The Supporting Information is available free of charge at https://pubs.acs.org/doi/10.1021/acsomega.1c04473.

Composition of 20 samples of natural gas (PDF)

■ AUTHOR INFORMATION

Corresponding Author

Yushuang Zhu − *State Key Laboratory of Continental Dynamics/Department of Geology, Northwest University, Xi'an 710069, China;* orcid.org/0000-0003-1938-2021; Email: Petroleum_gas@163.com

Authors

Jie He − *State Key Laboratory of Continental Dynamics/Department of Geology, Northwest University, Xi'an 710069, China*

Xiangdong Guo − *No. 1 Gas Production Plant, Yanchang Oil and Gas Exploration Company, Yan'an 716000, China*

Hongjun Cui − *No. 1 Gas Production Plant, Yanchang Oil and Gas Exploration Company, Yan'an 716000, China*

Kaiyu Lei − *No. 1 Gas Production Plant, Yanchang Oil and Gas Exploration Company, Yan'an 716000, China*

Yanyun Lei − *No. 1 Gas Production Plant, Yanchang Oil and Gas Exploration Company, Yan'an 716000, China*

Lin Zhou − *State Key Laboratory of Continental Dynamics/Department of Geology, Northwest University, Xi'an 710069, China*

Qinghai Liu − *State Key Laboratory of Continental Dynamics/Department of Geology, Northwest University, Xi'an 710069, China*

Linyu Liu − *State Key Laboratory of Continental Dynamics/Department of Geology, Northwest University, Xi'an 710069, China*

Complete contact information is available at: https://pubs.acs.org/10.1021/acsomega.1c04473

Notes

The authors declare no competing financial interest.

■ ACKNOWLEDGMENTS

This study was supported by the National Major Project (2017ZX05008-004-004-001). The authors would like to thank the editors and anonymous reviewers for their valuable suggestions for this paper.

■ NOTATIONS

Z deviation coefficient of natural gas;
V_R underground volume of natural gas, m^3;
V_{sc} volume of natural gas under surface conditions, m^3;
P_c wellhead casing pressure, MPa;
P_{ci} initial wellhead casing pressure, MPa;
P_{wf} bottom flow pressure, MPa;
P_{wfi} initial bottom flow pressure, MPa;
G_p cumulative production, 10^8 m^3;
$\overline{P}$ average formation pressure, MPa;
P_{wf} bottom flow pressure, MPa;
$\overline{Z}$ deviation factor of natural gas under average formation pressure;
Z_{wf} deviation factor of natural gas under bottom flow pressure;
$\overline{u_g}$ viscosity of natural gas under average formation pressure, mPa·s;
μ_{gwf} viscosity of natural gas under bottom flow pressure, mPa·s;
$\overline{C_g}$ compressibility of natural gas under average formation pressure, MPa^{-1};
C_{gwf} compressibility of natural gas under bottom flow pressure, MPa^{-1};
$\overline{P_{pss}}$ average formation pressure at the initial stage of the pseudo-steady-state, MPa;
$P_{wf\text{-}pss}$ bottom pressure at the initial stage of the pseudo-steady-state, MPa;
P_i initial formation pressure, MPa;
μ_g viscosity of natural gas, mPa·s;
C_g compressibility of natural gas, MPa^{-1};

λ $(\overline{u_g c_g})/(u_{gwf} c_{gwf})$

REFERENCES

(1) Nie, X.; Chen, J.; Yuan, S. Experimental Study on Stress Sensitivity Considering Time Effect for Tight Gas Reservoirs. *Mechanika* **2018**, *24*, 784−789.

(2) Ning, N.; Wang, H.-y.; Yong, H.; Liu, H.-l.; Hu, X.-j.; Zhao, Q.; Liu, D.-x. The unconventional natural gas resources and exploitation technologies in China. *Nat. Gas Ind.* **2009**, *29*, 9−12.

(3) Hirst, J. P. P.; Davis, N.; Palmer, A. F.; Achache, D.; Riddiford, F. A. The 'tight gas' challenge: appraisal results from the Devonian of Algeria. *Pet. Geosci.* **2001**, *7*, 13−21.

(4) Li, S. Z.; Qiao, D. W. Current Situation of Tight Sand Gas in China. *Adv. Mater. Res.* **2011**, *361-363*, 85−89.

(5) Sun, Z.; Shi, J.; Wang, K.; Miao, Y.; Zhang, T.; Feng, D.; Sun, F.; Wang, S.; Han, S.; Li, X. The gas-water two phase flow behavior in low-permeability CBM reservoirs with multiple mechanisms coupling. *J. Nat. Gas Sci. Eng.* **2018**, *52*, 82−93.

(6) Sun, Z.; Shi, J.; Zhang, T.; Wu, K.; Miao, Y.; Feng, D.; Sun, F.; Han, S.; Wang, S.; Hou, C.; Li, X. The modified gas-water two phase version flowing material balance equation for low permeability CBM reservoirs. *J. Pet. Sci. Eng.* **2018**, *165*, 726−735.

(7) Mattar, L.; Anderson, D.; Stotts, G. Dynamic material balance - oil- or gas-in-place without shut-ins. *J. Can. Pet. Technol.* **2006**, *45*, 7−10.

(8) Shengxiang, L. O.; Renchun, H. U.; Hongtao, L. I.; Yuchun, Y.; Guoping, L. I.; Zhenrui, B. A. Formation Mechanism of the Changxing Formation Gas Reservoir in the Yuanba Gas Field, Sichuan Basin, China. *Acta Geol. Sin.* **2011**, *85*, 233−242.

(9) Sun, Z.; Shi, J.; Wu, K.; Xu, B.; Zhang, T.; Chang, Y.; Li, X. Transport capacity of gas confined in nanoporous ultra-tight gas reservoirs with real gas effect and water storage mechanisms coupling. *Int. J. Heat Mass Transfer* **2018**, *126*, 1007−1018.

(10) Sun, Z.; Li, X.; Shi, J.; Zhang, T.; Sun, F. Apparent permeability model for real gas transport through shale gas reservoirs considering water distribution characteristic. *Int. J. Heat Mass Transfer* **2017**, *115*, 1008−1019.

(11) Sun, Z.; Shi, J.; Wu, K.; Li, X. Gas Flow Behavior through Inorganic Nanopores in Shale Considering Confinement Effect and Moisture Content. *Ind. Eng. Chem. Res.* **2018**, *57*, 3430−3440.

(12) Mattar, L.; McNeil, R. The "Flowing" Gas Material Balance. *J. Can. Pet. Technol.* **1998**, *37*, 1.

(13) Han, H. Y.; Wang, Z. Z.; Wang, L. C. The Application of Decision Tree Method to the Identification of Formation Types in Tight Gas Reservoirs. *Appl. Mech. Mater.* **2012**, *170-173*, 969−974.

(14) Han, G.; Liu, Y.; Sun, L.; Liu, M.; Gao, D.; Li, Q. Determination of pore compressibility and geological reserves using a new form of the flowing material balance method. *J. Pet. Sci. Eng.* **2019**, *172*, 1025−1033.

(15) Kanianska, R.; Gustafikova, T.; Kizekova, M.; Kovanda, J. Use of material flow accounting for assessment of energy savings: A case of biomass in Slovakia and the Czech Republic. *Energy Policy* **2011**, *39*, 2824−2832.

(16) Sun, Z.; Li, X.; Shi, J.; Yu, P.; Huang, L.; Xia, J.; Sun, F.; Zhang, T.; Feng, D. A semi-analytical model for drainage and desorption area expansion during coal-bed methane production. *Fuel* **2017**, *204*, 214−226.

(17) He, J.; Liu, X.; Zhu, X.; Jiang, T.; He, H.; Zhou, L.; Liu, Q.; Zhu, Y.; Liu, L. Water-flooding characteristics of lithologic reservoir in Ordos basin. *Sci. Rep.* **2021**, *11*, No. 2503.

(18) Feng, Z.; Liu, D.; Huang, S.; Gong, D.; Peng, W. Geochemical characteristics and genesis of natural gas in the Yan'an gas field, Ordos Basin, China. *Org. Geochem.* **2016**, *102*, 67−76.

(19) Guo, S.; Lyu, X.; Zhang, Y. Relationship between tight sandstone reservoir formation and hydrocarbon charging: A case study of a Jurassic reservoir in the eastern Kuqa Depression, Tarim Basin, NW China. *J. Nat. Gas Sci. Eng.* **2018**, *52*, 304−316.

(20) Hu, A.; Li, J.; Zhang, W.; Li, Z.; Hou, L.; Liu, Q. Geochemical characteristics and origin of gases from the Upper, Lower Paleozoic and the Mesozoic reservoirs in the Ordos Basin, China. *Sci. China, Ser. D: Earth Sci.* **2008**, *51*, 183−194.

(21) Guoyi, H.; Jin, L.; Xiuqin, S.; Zhongxi, H. The origin of natural gas and the hydrocarbon charging history of the Yulin gas field in the Ordos Basin, China. *Int. J. Coal Geol.* **2010**, *81*, 381−391.

(22) Peng, S. Q.; Zhao, W. C. The Adaptability Study for Developing Tight Gas Reservoirs Using Horizontal Wells. *Appl. Mech. Mater.* **2013**, *423-426*, 614−617.

(23) Schmoker, J. W. Resource-assessment perspectives for unconventional gas systems. *AAPG Bull.* **2002**, *86*, 1993−1999.

(24) Zhang, L.; Zhang, L. B.; Zhang, J. J.; Lan, F.; Deng, P. Calculation Methods of the Dynamic Reserves for Gas Wells in a Low-Permeability Gas Reservoir. *Appl. Mech. Mat.* **2013**, *295-298*, 3243−3248.

(25) Wang, Y.; Liu, L.; Zhang, Z.; Li, W.; Wang, Y.; Liu, X.; Wang, K.; Zhao, Y. Comparison of Ordos and Foreign Similar Basins and Prediction for Mesozoic Oil Reserves in Ordos Basin. *Geoscience* **2013**, *27*, 1244−1250.

(26) Zhang, J.-c.; Tang, X.; Jiang, S.-l.; Bian, R.-k. Natural gas accumulating and distribution spectra in clastic basins. *Nat. Gas Ind.* **2008**, *28*, 11−17.

(27) Shults, O. V. Method for calculating material balance of complex process flowcharts. *J. Math. Chem.* **2020**, *58*, 1281−1290.